

# Probing Reionization with the Cosmological Proximity Effect and High-Redshift Supernovae Rates

Andrei Mesinger

*Department of Astronomy, Columbia University, 550 West 120th Street, New York, NY 10027*

*E-mail: mesinger@astro.columbia.edu*

---

## Abstract

We develop and assess the potential of several powerful techniques, designed to investigate the details of reionization. First, we present a procedure to probe the neutral fraction,  $x_{\text{HI}}$ , using the Lyman alpha transmission statistics of high-redshift ( $z \gtrsim 6$ ) sources. We find that only tens of bright quasar spectra could distinguish between  $x_{\text{HI}} \sim 1$  and  $x_{\text{HI}} \lesssim 10^{-2}$ . A rudimentary application of such a technique on quasar SDSS J1030+0524 has yielded compelling evidence of a large neutral fraction ( $x_{\text{HI}} \gtrsim 0.2$ ) at  $z \sim 6$ . We also generate the observable, high- $z$  supernovae (SNe) rates and quantify the prospects of detecting the suppression of star-formation in low-mass galaxies at reionization from such SNe rates, specifically from those obtainable from the James Webb Space Telescope (*JWST*). Our analysis suggests that searches for SNe could yield thousands of SNe per unit redshift at  $z \sim 6$ , and be a valuable tool at studying reionization features and feedback effects out to  $z \lesssim 13$ .

*Key words:* cosmology, theory, supernovae, early Universe, quasars

---

## 1 Introduction

The epoch of cosmological reionization is a significant milestone in the history of structure formation. Despite recent observational break-throughs, the details of the reionization history remain poorly determined. The Sloan Digital Sky Survey (SDSS) has detected large regions with no observable flux in the spectra of several  $z \sim 6$  quasars (e.g. (1)). The presence of these Gunn-Peterson (GP) troughs set a lower limit on the volume weighted hydrogen neutral fraction of  $x_{\text{HI}} \gtrsim 10^{-3}$  (1), implying a rapid evolution in the ionizing background from  $z = 5.5$  to  $z \sim 6$  (e.g. (1)), and suggesting that we are witnessing the

end of the reionization epoch, with the IGM becoming close to fully neutral at  $z \sim 7$ . On the other hand, recent results from the Wilkinson Microwave Anisotropy Probe (WMAP) have uncovered evidence for a large optical depth to electron scattering,  $\tau_e \sim 0.17 \pm 0.04$  (2) in the cosmic microwave background anisotropies. This result suggests that the universe was already highly ionized at redshifts as high as  $z \sim 15 - 20$ . Various feedback mechanisms have been proposed to regulate the evolution of the ionization state of the IGM, with no clear consensus on a favored plausible physical model (e.g. (3)). It is evident that more tools designed to probe the reionization epoch would be of great value in pinning-down the reionization history and increasing our understanding of the early universe.

The rest of this contribution is organized as follows. In § 2 we discuss how the transmission statistics of high-redshift spectra can be used to place constraints on the neutral fraction and size of HII regions. In § 3, we describe how the extended dynamical range provided by the Lyman  $\alpha$  and Lyman  $\beta$  absorption allowed us to model the gross observed features of quasar SDSS J1030+0524. In § 4, we predict observable high-redshift SNe rates and asses their usefulness in the detection of reionization features. Finally, in § 5, we offer our conclusions. Most numerical estimates presented here assume standard concordance cosmological parameters,  $(\Omega_\Lambda, \Omega_M, \Omega_b, n, \sigma_8, H_0) = (0.73, 0.27, 0.044, 1, 0.9, 71 \text{ km s}^{-1} \text{ Mpc}^{-1})$ , consistent with the recent *WMAP* measurements. Unless stated otherwise, all lengths are quoted in comoving units.

## 2 Mock Spectral Analysis

In principle, the quasar's absorption spectrum contains a full record of the neutral fraction as a function of position along the line of sight. Since high-redshift sources sit in their own highly ionized Strömngren spheres, the total Lyman  $\alpha$  optical depth at a given observed wavelength,  $\lambda_{\text{obs}}$ , can be written as the sum of contributions from inside and outside the Strömngren sphere,  $\tau_{\text{Ly}\alpha} = \tau_R + \tau_D$ . These two contributions are shown in Figure 2, originating from a hydrodynamical simulation (further details of the simulation can be found in (5)). The residual neutral hydrogen inside the Strömngren sphere resonantly attenuates the quasar's flux at wavelengths around  $\lambda_\alpha(1+z)$ , where  $\lambda_\alpha = 1215.67 \text{ \AA}$  is the rest-frame wavelength of the Lyman  $\alpha$  line center. As a result,  $\tau_R$  is a fluctuating function of wavelength (solid curve), reflecting the density fluctuations in the surrounding gas. In contrast, the damping wing of the absorption,  $\tau_D$ , is a relatively smooth function (dashed curve), because its value is averaged over many density fluctuations. The damping wing optical depth is a strong function of the size of the Strömngren sphere,  $R_S$ , and the hydrogen neutral fraction outside the Strömngren sphere,  $x_{\text{HI}}$ .

Although there is a wealth of information in these two components, it is systematically challenging to separate them and hence extract relevant parameters. In (5), we study the feasibility of statistically extracting such parameters from high redshift spectra. The free parameters in our analysis are  $R_S$  and  $x_{\text{HI}}$ . Note that changing  $R_S$  moves the dashed ( $\tau_D$ ) curve left and right, while changing  $x_{\text{HI}}$  moves this curve up and down in Figure 2.

The analysis can be summarized as the following. We start with a simulated observed spectrum, generated using a randomly chosen line of sight (LOS) from a cosmological hydrodynamic simulation. Then we guess values for the radius of the Strömgen sphere,  $R'_S$ , and the IGM hydrogen neutral fraction,  $x'_{\text{HI}}$ . Next we approximate the amplitude of the source’s intrinsic emission,  $A'$ , implied by the choices of  $R'_S$  and  $x'_{\text{HI}}$ , using the red side of the Lyman  $\alpha$  line where resonance absorption can be neglected. From the observed spectrum, we divide out the assumed intrinsic emission ( $A' \times \textit{known spectral shape}$ ), and the assumed damping wing flux decrement,  $e^{\tau_D(\lambda_{\text{obs}}, R'_S, x'_{\text{HI}})}$ , calling the result  $S'(\lambda_{\text{obs}})$ . If our choices of  $R'_S$  and  $x'_{\text{HI}}$  were correct,  $S'(\lambda_{\text{obs}})$  should represent the resonance absorption flux decrement alone. Hence, we compare a histogram of the implied resonance optical depths,  $-\ln[S'(\lambda_{\text{obs}})]$ , to the known histogram of resonance optical depth (obtained from the simulation). We then repeat this procedure with different choices of  $R'_S$  and  $x'_{\text{HI}}$ , finding the ones whose implied resonance optical depths most closely match the known histogram.

A few of the resulting histograms are shown in Figure 1. The template distribution of resonance optical depths obtained from our simulation is shown in the top left panel. Distributions derived from our inversion analysis explained above are shown in the other panels, with the correct parameter choice in the top right and incorrect choices in the bottom two panels. We test the hypothesis that the top right, bottom left and bottom right histograms (among many others in parameter space) were drawn from the distribution in the top left. We find that the top right panel is consistent with being drawn from the distribution in the top left, and that the bottom panels are not.

Additionally, we have explicitly incorporated into our analysis an error in the intrinsic emission template, consisting of either an uncertainty in its spectral power-law index, or Gaussian, uncorrelated, pixel-to-pixel variations at each wavelength. With both of these errors, we find that a neutral universe can be statistically distinguished from a  $x_{\text{HI}} = 0.008$  universe in our parameter space, using tens of bright quasars, a sample that can be expected by the completion of the Sloan Digital Sky Survey. Alternatively, similar statistical constraints can be derived from the spectra of several hundred sources that are  $\sim 100$  times fainter. For example, the Large-aperture Synoptic Survey Telescope (LSST) should be able to deliver many new faint quasars that could serve as targets for low-resolution spectroscopy. Furthermore, if the size of the source’s Strömgen sphere can be independently constrained to within  $\sim$

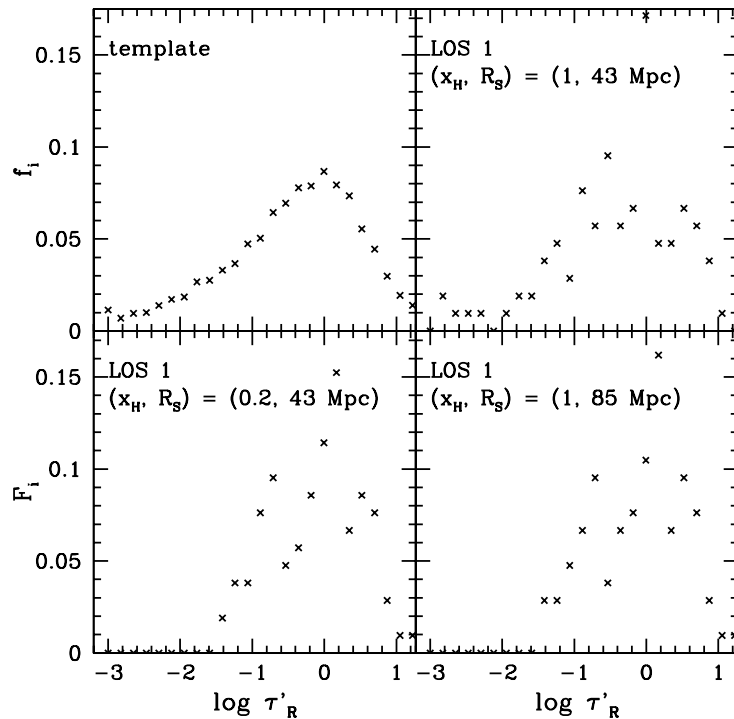


Fig. 1. Histogram of the template distribution  $\tau_R$  (*top left*), and histograms of the derived  $\tau'_R$  distribution:  $(x_{\text{HI}}, R_S) = (1, 43 \text{ Mpc})$  (*correct values top right*),  $(x_{\text{HI}}, R_S) = (0.2, 43 \text{ Mpc})$  (*bottom left*),  $(x_{\text{HI}}, R_S) = (1, 85 \text{ Mpc})$  (*bottom right*). We test the hypothesis that the top right, bottom left and bottom right histograms (among many others in parameter space) were drawn from the distribution in the top left. We find that the top right panel is consistent with being drawn from the distribution in the top left, and that the bottom panels are not.

10% (such as with the method presented in (6)), the analysis presented here can distinguish between sources embedded in an IGM with  $10^{-3} < x_{\text{HI}} < 1$ , using a single source. We plan to perform such analysis on the current sample of high-redshift sources.

### 3 Case of SDSS J1030+0524

The challenges discussed above in extracting relevant parameters from high-redshift spectra are partially aggravated by the limited dynamical range probed by observations. For example, the sharp rise in  $\tau_D$  at wavelengths  $\lambda_{\text{obs}} \lesssim 8720 \text{ \AA}$  in Fig. 2 is a unique feature of the boundary of the HII region, and corresponds to absorption of photons redshifting into resonance outside of the Strömgren sphere. The detection of this feature has generally been regarded as challenging: since the quasar's flux is attenuated by a factor of  $\exp(-\tau_{\text{Ly}\alpha})$ , an exceedingly large dynamical range is required in the corresponding flux

measurements. However, in (6) we show that simultaneously considering the measured absorption in two or more hydrogen Lyman lines can provide the dynamical range required to detect this feature.

The observational input to our analysis is the deepest-exposure absorption spectrum of SDSS J1030+0524 available to date (7). The flux detection threshold in the Lyman  $\alpha$  and Lyman  $\beta$  regions of this spectrum correspond to total Lyman  $\alpha$  optical depths of  $\tau_{\text{lim(Ly}\alpha)} \approx 6$  and  $\tau_{\text{lim(Ly}\beta)} \approx 11$  respectively. To summarize the implied constraints, we have divided the spectrum into three different regions, shown in Figure 2. In Region 1, with  $\lambda_{\text{obs}} \geq 8752.5 \text{ \AA}$ , the detection of flux from SDSS J1030+0524 corresponds to the *upper* limit on the total optical depth  $\tau_{\text{Ly}\alpha} < 6$ . Region 2, extending from  $8725.8 \text{ \AA} \leq \lambda_{\text{obs}} < 8752.5 \text{ \AA}$ , is inside the Lyman  $\alpha$  trough, but outside the Lyman  $\beta$  trough. Throughout this region, the data requires  $6 \lesssim \tau_{\text{Ly}\alpha} \lesssim 11$ . Region 3, with  $\lambda_{\text{obs}} < 8725.8 \text{ \AA}$  has a *lower* limit  $\tau_{\text{Ly}\alpha} \geq 11$ . As defined, each of these three regions contains approximately eight pixels in the spectrum of SDSS J1030+0524.

We modeled the absorption spectrum of SDSS J1030+0524, attempting to match these gross observed features. We extracted density and velocity information from 100 randomly chosen lines of sight (LOSs) through the simulation box (described in (5)). The density and velocity distributions are biased near the density peaks where a quasar may reside. However, the spectral region of interest lies well outside these biased regions, which, in the case of high-redshift quasars, extends only to  $\lesssim 1$  proper Mpc, on average (8). The use of randomly chosen LOSs is therefore an accurate statistical representation of the expected density and velocity fields. Along each LOS, we computed the Lyman  $\alpha$  absorption as a function of observed wavelength.

In this analysis, we had three free parameters: (i) the size of the ionized region ( $R_S$ ); (ii) the fraction of neutral hydrogen outside it ( $x_{\text{HI}}$ ); (iii) the QSO's ionizing luminosity ( $L_\nu$ ). To understand the significance of these three parameters, note that changing  $R_S$  moves the dashed ( $\tau_D$ ) curve left and right, while changing  $x_{\text{HI}}$  moves this curve up and down in Figure 2; changing  $L_\nu$  corresponds to moving the solid ( $\tau_R$ ) curve up and down. Values of  $x_{\text{HI}} < 1$  imply the existence of a background flux of ionizing radiation, with an ionization rate of  $\Gamma_{12} \approx 10^{-5} x_{\text{HI}}^{-1} \times 10^{-12} \text{ s}^{-1}$ . For consistency, we add this constant background flux to that of the quasar (the latter dropping as  $r^{-2}$  with distance), somewhat reducing the neutral hydrogen fraction inside the ionized region.

We evaluated  $\tau_R$  and  $\tau_D$  for each LOS in our simulation and for every combination of  $R_S$ ,  $x_{\text{HI}}$ , and  $L_\nu$ , attempting to match the gross features explained above. In order to be conservative, we allowed up to two pixels in each region to lie outside the allowed range of Lyman  $\alpha$  optical depths; each LOS that had more than two pixels fail the above criteria in any of the three regions

was rejected. We find that a more stringent criterion of allowing only a single ‘faulty’ pixel would strengthen our conclusions.

The procedure outlined above turns out to provide tight constraints on all three of our free parameters *simultaneously*. The radius of the Strömngren sphere is limited to  $42 \text{ Mpc} \leq R_S \leq 47 \text{ Mpc}$ , close to the previously estimated lower limits (9; 10). We also find evidence that the IGM was significantly neutral at  $z \sim 6$ , with a  $\sim 1 \sigma$  lower limit of  $x_{\text{HI}} \gtrsim 0.17$ . This result is derived from the observed sharpness of the boundary of the HII region alone, and relies only on the gross density fluctuation statistics from the numerical simulation. In particular, it does not rely on assumptions about the mechanism for the growth of the HII region. Finally, we find an emission rate of ionizing photons per second of  $(5.2 \pm 2.5) \times 10^{56} \text{ photons sec}^{-1}$ , which is between 2 – 10 times lower than expected (11; 12), strengthening arguments that reionization at  $z \sim 6$  is caused by the radiation from early stars, rather than bright quasars (13).

Our findings represent the first detection of the boundary of a cosmological HII region, and have several important implications. As was previously mentioned in § 2, tight constraints on the hydrogen neutral fraction can be extracted directly from the Lyman  $\alpha$  absorption spectrum alone (5), but this requires tens of spectra to be statistically significant when  $R_S$  is not known. Incorporating an independent limit on  $R_S$ , such as the one obtained from this method, can reduce the number of required spectra to *one*. Tight constraints on  $x_{\text{HI}}$  have also recently been obtained by adopting a proper size of  $R_S \approx 4.5 \text{ Mpc}$  for SDSS J1030+0524, together with an estimate of its lifetime (14). Our direct determination of the Strömngren sphere size is only slightly larger than the previously adopted value, lending further credibility to this conclusion. The sharp boundary we detect also constrains the hardness of the ionizing spectrum of SDSS J1030+0524. We infer here a rise in the neutral fraction over a redshift interval of  $\Delta z \sim 0.02$ , corresponding to a proper distance of  $\sim 1.2 \text{ Mpc}$ . The thickness of the Strömngren surface is approximately given by the mean free path of the typical ionizing photon. In order for this mean free path not to significantly exceed the observed thickness, the mean energy of the ionizing photon emitted by SDSS J1030+0524 must be  $< 230 \text{ eV}$ . This is an interesting limit, implying that the effective slope of the ionizing spectrum of this source above  $E = 13.6 \text{ eV}$  is softer than  $-d \ln L_\nu / d \ln \nu = 1.07$ .

In the future, given a larger sample of quasars at  $z > 6$ , it will be possible to use the method presented here to search for sharp features in the absorption spectrum from intervening HII regions, not associated with the background source itself. We plan to study the utility of this approach in a future paper. For such external HII regions that happen to intersect the line of sight, both the red and the blue sides of each GP trough can, in principle, be detected, and can yield two separate measurements of the ionized fraction at different

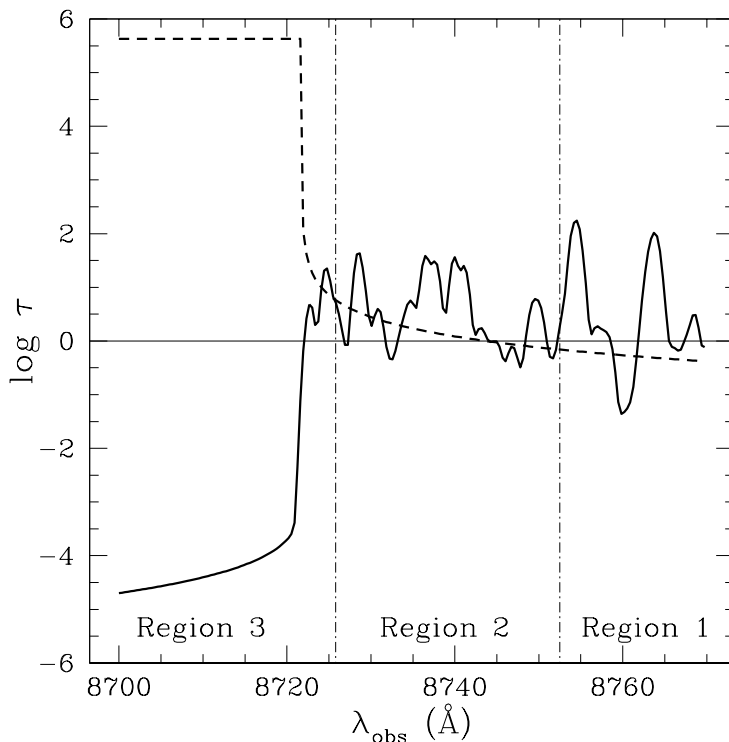


Fig. 2. Model from a hydrodynamical simulation for the optical depth contributions from within ( $\tau_R$ ) and from outside ( $\tau_D$ ) the local ionized region for a typical line of sight towards a  $z_s = 6.28$  quasar embedded in a fully neutral, smooth IGM, with  $R_S = 44$  Mpc and  $f_{\text{ion}} = 1$ . The *dashed curve* corresponds to  $\tau_D$ , and the *solid curve* corresponds to  $\tau_R$ . The total Lyman  $\alpha$  optical depth is the sum of these two contributions,  $\tau_{\text{Ly}\alpha} = \tau_R + \tau_D$ . The *dashed-dotted lines* demarcate the three wavelength regions used for our analysis described in the text. In our analysis, the optical depths are averaged over  $3.5 \text{ \AA}$  wavelength bins, which decreases the fluctuation of  $\tau_R$ . For reference, the redshifted Lyman  $\alpha$  wavelength is at  $8852 \text{ \AA}$ .

points along the line of sight. The Universe must have gone through a transition epoch when HII regions, driven into the IGM by quasars and galaxies, partially percolated and filled a significant fraction of the volume. The detection of the associated sharp features in future quasar absorption spectra will provide a direct probe of the the 3D topology of ionized regions during this crucial transition epoch. Deep surveys equipped with sufficiently red filters (with instruments such as those being carried out by the VLT, and ultimately with deep surveys covering a significant portion of the sky, such as the survey proposed with the LSST; (15)) will be able to deliver a large sample of bright  $z > 6$  quasars needed for such studies.

## 4 High-Redshift SNe Rates

During reionization, the ionizing background radiation heats the IGM and could dramatically suppress gas accretion and star formation in low-mass halos. As a result, reionization may be accompanied by a drop in the star-formation rate (SFR) and the corresponding supernovae rate (SNR). The size of the drop is uncertain, since the ability of the gas in low-mass halos to cool and self-shield against the ionizing radiation is poorly constrained at high redshifts. The redshift and width of the drop are also uncertain as the details of reionization are also unknown. In (16), we construct the observable, high- $z$  SNe rates, and analyze the prospects of detecting a reionization feature with future SNe observations, specifically those obtainable with *JWST*.

Such a drop in the SFR could be detected in the high-redshift extension of the 'Madau' diagram (e.g. (17)), by directly counting faint galaxies (18). However, these galaxies are dangerously close to the detection thresholds of forthcoming instruments, making a reionization feature detectable only in very optimistic scenarios. Alternatively, by analyzing the Lyman  $\alpha$  absorption spectra of SDSS quasars, (19) suggest that we may already have detected a drop in the SFR at  $z \sim 6$ , through the non-monotonic evolution of the mean IGM opacity. In order to improve on this current, low signal-to-noise result, many deep, high-resolution, high- $z$  spectra of bright quasars would be required. Other events that may trace out the early SFR, such as gamma-ray bursts (GRBs) and SNe, could be better suited to detect the reionization drop, as they are bright, and could be used as tracers of the SFR in arbitrarily faint host galaxies, out to redshifts higher than the host galaxies themselves. Unfortunately, while GRBs are bright, they are rare. Based on the expected *Swift* GRB detection rates (e.g. Figure 6 in (20)), a drop in the GRB rate associated with reionization could be detected only at very low,  $\sim 1\sigma$ , significance, and only if reionization occurred at  $z_{\text{re}} \lesssim 7 - 10$ . On the other hand, SNe have the benefits of being both very bright (compared to galaxies at the very faint end of the luminosity function), and occurring much more frequently (compared to GRBs).

There have been several previous studies of the expected early SNR. However, these either did not focus on the expected rates at redshifts beyond reionization (e.g (21)), focused exclusively on very high- $z$  rates from the first generation of metal-free stars (22), and/or did not address the impact of reionization on the SFR (e.g. (23; 24)). Likewise, previous theoretical predictions of the high-redshift SFR (e.g. (18)) assumed a fixed degree of suppression due to reionization, matching numerical simulations which did not include self-shielding (25). The main distinctions here are that we compute the expected SNe rates at a wide range of redshifts and we allow various degrees of photoionization heating feedback. We also supplement the standard halo-based estimates of the SFR with a more elaborate estimate of the corresponding



observable SNR, utilizing the observed properties of low- $z$  SNe.

We assume that the SFR at high redshift traces the formation rate of dark matter halos. We vary the redshift, width and size of the drop in the SFR. We assume that 50% of the high-redshift SNe are Type IIP and 50% are Type IIL. We make use of the observed properties of local SNe, such as their lightcurves (26), spectra (27), and peak magnitude distributions (28), to predict the corresponding number of detectable SNe as a function of redshift. Specifically, we consider *JWST*, a 6m diameter space telescope, scheduled for launch in 2013. The relevant instrument on *JWST* is NIRcam, a near-infrared imaging detector with a FOV of  $2.3' \times 4.6'$  and simultaneous exposures in two filters.

We find that 4 – 24 SNe may be detectable from  $z \gtrsim 5$  at the sensitivity of 3 nJy (requiring  $10^5$  s exposures in a  $4.5 \mu\text{m}$  band) in each  $\sim 10 \text{ arcmin}^2$  *JWST* field. In a hypothetical one year survey (or a collection of  $\sim$  hundred repeated exposures), we expect to detect up to thousands of SNe per unit redshift at  $z \sim 6$ . Our results imply that, for most scenarios, high-redshift SNe observations can be used to detect reionization features out to  $z \sim 13$ , as well as set constraints on the photoionization heating feedback on low-mass halos at the reionization epoch. Specifically, for a wide range of scenarios at  $z_{\text{re}} \lesssim 13$ , the drop in the SNR due to a sharp feature in the reionization history can be detected at  $S/N \gtrsim 3$  with only tens of deep *JWST* exposures. In cases with strong negative feedback, the drop in the SNR can be detected if it's spread out over  $\Delta z_{\text{re}} \lesssim 4$ ; less optimistic scenarios require  $\Delta z_{\text{re}} \sim 1 - 2$ . Even in the case of a more extended reionization history, fairly sharp features are likely, which could leave detectable signatures in the SNR (see Fig. 9 in (16), and associated discussion). Our results therefore suggest that future searches for high- $z$  SNe could be a valuable new tool, complementing other techniques, to study the process of reionization, as well as the feedback mechanism that regulates it.

## 5 Conclusions

We have developed several useful tools designed to probe reionization. The main implications of these works can be summarized as follows.

- The cosmological proximity effect can be used to study imprints of the host environment properties on the source's spectra; specifically, a neutral fraction of  $x_{\text{HI}} = 1$  and be distinguished from  $x_{\text{HI}} \lesssim 0.01$  with only tens of bright QSO spectra (or  $\sim$  hundreds of spectra which are 100 times fainter), in the presence of emission uncertainties of  $\sim 20\%$ .
- The spectral analysis of QSO SDSS J1030+0524 suggests that the Universe (or at least a large part of it) is very neutral at  $z \sim 6.2$ , with  $x_{\text{HI}} \gtrsim 0.2$ .

- The ionizing luminosity of SDSS J1030+0524 is a factor of  $\sim 2$ –10 lower than expected, strengthening arguments against quasar-dominated reionization.
- Disparate Lyman line absorption statistics can probe ionization topology.
- The sharpness of the Strömngren sphere boundary can be used to constrain the X-ray contribution to the quasar’s intrinsic emission.
- Future instruments, such as *JWST*, can yield many high- $z$  SNe; specifically, 4 – 24 SNe/field may be detectable from  $z \gtrsim 5$  at the sensitivity of 3 nJy.
- High- $z$  SNe can be used to detect reionization features out to  $z \lesssim 13$ .

I thank my advisor, Zoltán Haiman, and my collaborators Renyue Cen and Benjamin Johnson for permission to draw on joint work.

## References

- [1] X. Fan, *et al.*, *AJ* **123**, 1247 (2002).
- [2] C. L. Bennett, *et al.*, *Astrophys. J. Suppl.* **148**, 1 (2003).
- [3] Z. Haiman and G. .P. Holder, *Astrophys. J.* **595**, 1 (2003).
- [4] D. N. Spergel, *et al.*, *Astrophys. J. Suppl.* **148**, 175 (2003).
- [5] A. Mesinger, Z. Haiman, and R. Cen, *Astrophys. J.* **613**, 23 (2004).
- [6] A. Mesinger and Z. Haiman, *Astrophys. J.* **611**, 69 (2004).
- [7] R. L. White, *et al.*, *AJ* **126**, 1 (2003).
- [8] R. Barkana and A. Loeb, *Astrophys. J.* **601**, 64 (2004).
- [9] P. Madau and M. J. Rees, *Astrophys. J.* **542**, 69 (2000).
- [10] R. Cen and Z. Haiman, *Astrophys. J.* **542**, 75 (2000).
- [11] M. Elvis, *et. al.*, *Astrophys. J. Suppl.* **95**, 1 (1994).
- [12] R. C. Telfer, W. Zheng, and G. A. Kriss, *AJ* **565**, 773 (2002).
- [13] M. Dijkstra, Z. Haiman, and A. Loeb, *Astrophys. J.* **613**, 646 (2004).
- [14] J. S. B. Wyithe, and A. Loeb, *Nature* **427**, 815 (2004).
- [15] J. A. Tyson, *Proc. SPIE Int. Soc. Opt. Eng.* **4836**, 10 (2003).
- [16] A. Mesinger, B. D. Johnson, and Z. Haiman, preprint [arXiv:astro-ph/0505110].
- [17] P. Madau *et al.*, *MNRAS* **283**, 1388 (1996).
- [18] R. Barkana and A. Loeb, *Astrophys. J.* **539**, 20 (2000).
- [19] R. Cen and P. McDonald, *Astrophys. J.* **570**, 457 (2002).
- [20] A. Mesinger, R. Perna, and Z. Haiman, *Astrophys. J.* **623**, 1 (2005).
- [21] P. Madau, M. della Valle, and N. Panagia, *MNRAS* **297**, 17 (1998).
- [22] J. H. Wise and T. Abel, preprint [arXiv:astro-ph/0411558].
- [23] J. Miralda-Escude and M. J. Rees, *Astrophys. J.* **478**, 57 (1997).
- [24] T. Dahlén and C. Fransson, *AAP* **350**, 349 (1999).
- [25] A. A. Thoul and D. H. Weinberg, *Astrophys. J.* **465**, 608 (1996).
- [26] J. B. Doggett and D. Branch, *AJ* **90**, 2303 (1985).
- [27] E. Baron, *et al.*, *Astrophys. J.* **545**, 444 (2000).
- [28] D. Richardson, *et al.*, *AJ* **123**, 745 (2002).